

We are IntechOpen, the world's leading publisher of Open Access books Built by scientists, for scientists

6,900

Open access books available

185,000

International authors and editors

200M

Downloads

Our authors are among the

154

Countries delivered to

TOP 1%

most cited scientists

12.2%

Contributors from top 500 universities



WEB OF SCIENCE™

Selection of our books indexed in the Book Citation Index
in Web of Science™ Core Collection (BKCI)

Interested in publishing with us?
Contact book.department@intechopen.com

Numbers displayed above are based on latest data collected.
For more information visit www.intechopen.com



Laser welding process: Characteristics and finite element method simulations

Yannick Deshayes

*University of Bordeaux 1-IMS Laboratory
France*

1. Context and objectives

Expertise of packaging for optoelectronic components requires the solution of optical, mechanical and electrical problems in the same way. The purpose of this study is to present three-dimensional simulations using finite element method (FEM) of thermomechanical stresses and strains in transmitter Laser modules induced by Nd:YAG crystal Laser welds on main sub-assembly Laser submount. Non-linear FEM computations, taking into account of experimental $\sigma(\epsilon)$ measured curves, show that Laser welding process can induce high level of strains around the Laser welding zone, bearing the Laser diode, responsible of an optical axis shift and a gradual drop of the optical power in relation with relaxation of accumulated stresses in the sub-assembly (Sherry and al., 1996). Typical stresses are close to 160 MPa with drift about 5 MPa with the dispersion of energy level of laser Nd : YAG beam. The introduction of both material and process dispersion in order to evaluate their impact on product life time distribution has been taking into account. Thermal cycles (-40°C/+85°C VRT) are used to estimate the robustness of the technology assembly. Previous paper demonstrated that Laser submount near laser welding zones is the most sensitive part of optical system (Deshayes and al., 2003). The gradual changes of stresses distribution from the laser welding process and after thermal cycles are estimate using FEM. Experimental analyses were also conducted to correlate simulation results and monitor the output optical power of Laser modules after 500 thermal cycles.

The development of high bandwidth single mode fibre optics communication technologies coupled with the availability of transmitter components for wavelength multiplexing has created a revolution in the transmission technology during the last fifteen years. These performances can be reached by packaging interface and control circuits with the optical chips leading to the concept of high reliable technically-advanced Laser modules. Reduced cost, low consumption, hermetical and highly efficient optical coupling between the Laser diode and the single-mode fibre associated to a mechanical stability are some of the key issues. Moreover, packaging of such systems requires the resolution of optical, thermomechanical and electrical problems.

These problems are often highly interactive and the stability of optoelectronic devices is still an essential factor to ensure high bandwidth data transmission, acceptable bit-error rate and develop reliable solutions. In actual telecommunication applications, photonic systems involve a non direct mechanical alignment between the laser diode and the optical fibre

(Deshayes and al., 2003; Breedis and al., 2001). Generally, one or two lens are used to for this optical alignment. For instance, mechanical stability requires tolerances less than 1 μm to avoid a power change higher than 10 %, which must be consistent during the lifetime of the module and across the temperature range.

For optical alignment, three primary techniques have been developed to align and connect the light-emitter to the optical fibre associated with different package configurations (Jang, 1996; Song and al., 1996) :

- Solder with V-groove,
- Epoxies,
- Nd:YAG Laser welds.

It has been already demonstrated that Nd:YAG Laser welding technique is the most effective method to satisfy performances criteria previously described. Due to inherent advantages, a growing number of communication systems integrators are requesting Laser welded packages for their end-users. However the challenge of containing the solidification shrinkage caused by the light-metal interaction during the welding process, resulting in a weld shift leading to the reduction of coupling efficiency and device throughput stability (Song and al., 1996).

Standard qualification procedures, in particular power drift monitoring, must be conducted to validate the system with respect to tolerances through temperature cycling or storage temperature characterizing the limits and the margins of the technology. Actual standards tend to be 500 cycles in the temperature range $-40^{\circ}\text{C}/+85^{\circ}\text{C}$ without failures (Goudard and al., 2002). These ageing tests are generally realized in order to evaluate all the parameters in relation with failure distribution but more than one hundred modules must be performed during several thousands hours mixing different life test conditions. These results can allow determining the robustness of the technology but due to a high complexity of the package, cannot give accurate information on the failure origin, which is responsible of the optical power drift. To face qualification challenges, new processes are now being proposed focusing on reliability concerns at the early stage of the product development. In this approach, the qualification is considered as a long-term process rather than a final exam at the end of the development (Goudard and al., 2002). Based on environmental and functional specifications, the product development can start with a technical risk analysis phase. This phase aims at pointing out the major risks for a given product design. In this case, physical simulation (thermal and/or mechanical) represents an attractive tool to assess and weigh up the risk criticality (Mcleod and al., 2002).

The purpose of this paper deals with results achieved from nonlinear thermomechanical simulations using finite-element method (FEM) of a direct modulation 1.55 μm Laser module (10 mW) for telecommunication applications. This study completes the thermomechanical studies in laser diodes module emitting at 1550 nm (Mcleod and al., 2002).

This paper will be developed in three main parts:

- description of the methodology to implement in FEM the Nd:YAG Laser welding using electro-thermal analogies,
- calculations of stresses and strains after Laser welding process between the Laser diode platform and the lens holder taking into account of experimental process parameters,

- impact of calculated strains on optical misalignment (angular deviation of the optical axis) with respect to dispersion process.

2. Laser welding model for FEM

2.1 Theory of laser material interaction

a. Spatial structure and coherent

The structure of laser wave is critical for understand the thermal flow during the laser welding process. This part presents the basic structure of laser wave.

The spatial structure of laser wave can be expressed considering the electric field $E(x, y, z)$ by equation (1):

$$E(x, y, z) = E_0 \left[\frac{\omega_0}{\omega(z)} \right] \exp - i \left(k \left[z + \frac{r_{\perp}^2}{2R(z)} \right] - \phi(z) \right) \times \exp \left[\frac{r_{\perp}^2}{\omega^2(z)} \right] \quad (1)$$

With $r_{\perp}^2 = x^2 + y^2$: transversal radius, $E_0 = E(x, y, 0)$: transversal electric field, $\omega^2(z) = \omega_0^2 \left[1 + (\lambda z / \pi \omega_0^2)^2 \right]$: the radial extension of the laser beam, $R(z) = z \left[1 + (\pi \omega_0^2 / \lambda z)^2 \right]$: curvature radius of the laser beam.

The geometry of the laser beam can be represented by the fig 1.

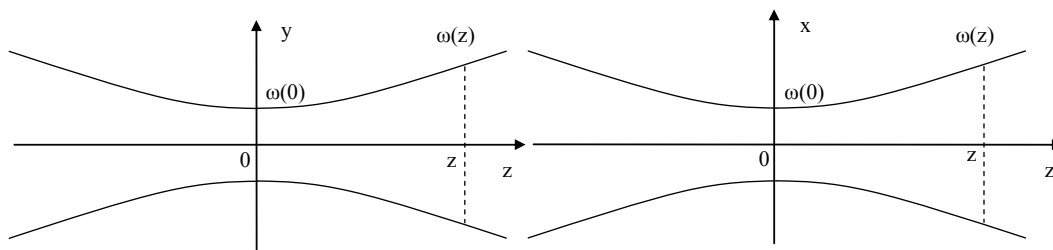


Fig. 1. Geometry of the transversal structure for the Gaussian propagation

The ω_0 correspond to the beam waist that is critical for a laser welding process. The beam waist has been experimentally explored on the optoelectronic module as the fig. 2 shown. There are two different zones in the laser welded joints: the melting zone ($T_{liq} < T < T_{max}$) and the Heat Affected Zone (HAZ). The melting zone corresponds to the structure of the laser beam and we observe the beam waist equal to 200 μm in the case presented in fig.2. The quasi circular lines located in HAZ ($T_{lim} < T < T_{liq}$) correspond to the isothermal line. The laser beam intensity is described by a Gaussian Law as proposed by equation (2):

$$T(r) = T_{lim} + (T_{max} - T_{min}) \exp \left(- \frac{r_{\perp}^2}{\omega_0^2} \right) \quad (2)$$

The T_{max} is the maximal temperature estimated at 1823 K, $T_{min} = 600$ K is the minimal temperature corresponds to the solidification of material and T_{liq} is the limit between liquid-solid phase temperature. In this condition, the material is not liquid but melting with liquid

and solid and the Young Modulus is 100 time less than solid material. This condition explain the HAZ until diameter around 800 μm

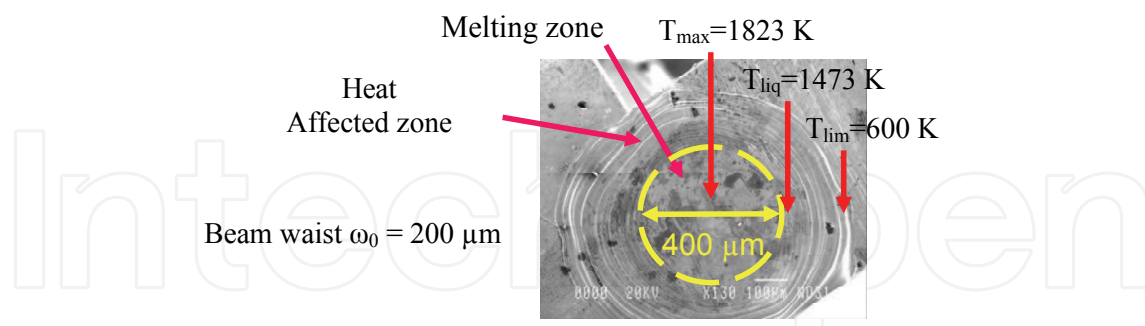


Fig. 2. Geometry of the transversal structure for the Gaussian propagation

The main objective of the FEM model is to simulate the same phenomenon but the great difficulty is to *apply Gaussian thermal flux on the laser welded zone*.

2.2 Methodology for build FEM model

a. Pattern geometry

Actual graphic performances of the simulator allow, without difficulty, to building a complex geometric model generally coming from the design plans of the considered system. The most important difficulty resides in the dividing of the geometric model in finite elements. It is necessary to follow a procedure of model building very strict allowing to insure, in the final, to obtain an optimum pattern.

b. Finite elements definition

The FEM consist to find an approximate solution of exact solution with field of discretization defined on sub-domain Ω_i of global domain Ω . The sub-domain Ω_i have been build considering equation (3).

$$\bigcup_{i=1}^{i=n} \Omega_i = \Omega \text{ and } \Omega_i \cap \Omega_j = \emptyset \quad \forall i \neq j \quad (3)$$

Fields $\tilde{f}(M, t)$, defined for each sub domain Ω_i is called local field family and is generally defined as polynomial function. The global field family $\tilde{F}(M, t)$, obtained by superposition of local fields, is called interpolation function space of domain Ω .

The field for each sub-domain Ω_i is determined by a finite number of value of field (or value of first order derivation) in arbitrary points in the sub-domain and called nodes. The local field is an interpolation between the values associated to nodes. The sub-domain with its interpolation is called element.

Find a solution by finite element method consists in the determination of local field that can be attributed for each sub-domain for the global field $\tilde{F}(M, t)$ calculated by superposition of local field is close to real solution of the problem.

c. Elements and geometry combination

The elements constitute for software resolution a little volume element for integration or differential equation resolution. In international reference, it exist only three different geometric references: Cartesian, geometrical and cylindrical. In Finite element model, the single element can be associated as an elementary discrete volume $d^3\tau$.

For example, we consider Cartesian representation. In this case, the elementary volume is a parallelepiped element defined by equation (4):

$$d^3\tau = dx \cdot dy \cdot dz \quad (4)$$

and represented by fig. 3.

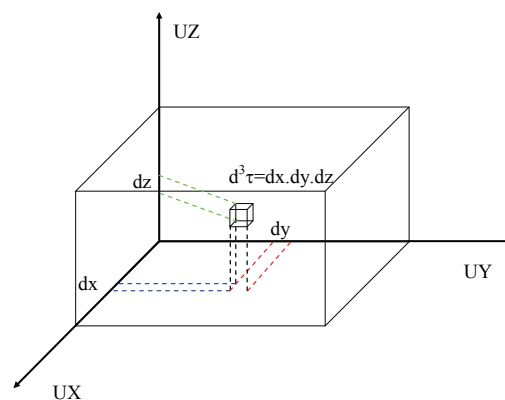


Fig. 3. Cartesian geometric reference and elementary volume

For cylindrical and spherical representation, the finite element can be adjusted to form a single elementary volume allowing to describe respectively cylindrical or spherical system. The accuracy of the simulation results for system considered is, in part, related to both element design and their number.

d. Physical associated to element

➤ Mechanical elements

Elements of this type require material's features properties listed below: Young modulus, poisson ratio, plastic modulus, coefficient thermal dilatation, material density. This element allows to perform linear or non linear simulation taking into account of non-linearity of materials (plastic deformation, creep,...). The non linearity is also induced by geometry structure as contact of area to simulate pivot link for example.

➤ Thermal elements

Elements of this type require material's features properties listed below: thermal conductivity, material density, heat capacity, and enthalpy for material phase change. This element allows to perform linear or non linear simulation taking into account of non-linearity of materials (phase change).

➤ Coupled field elements

Coupled field associate in same time the mechanical, thermal, electrical and magnetic simulations. In this case, the material behaviour is considered as linear and all

simulations are performed in same time. In the case where it is necessary to perform thermal and mechanical simulations, for example, on the structure with non-linear material properties, the solution is to perform, in the first time the thermal simulation and in the second time to execute the mechanical simulation. The thermal simulation became boundary conditions of the mechanical simulation for this example.

e. Geometry of elements

➤ Regular elements

Elements are also characterized by their geometry in Cartesian coordinates (x, y, z) , cylindrical (ρ, θ, z) and spherical (ρ, θ, φ) for three dimensional simulation. Generally this kind of elements is constituted by 8 or 16 nodes as it indicates in fig. 4 and is named regular elements.

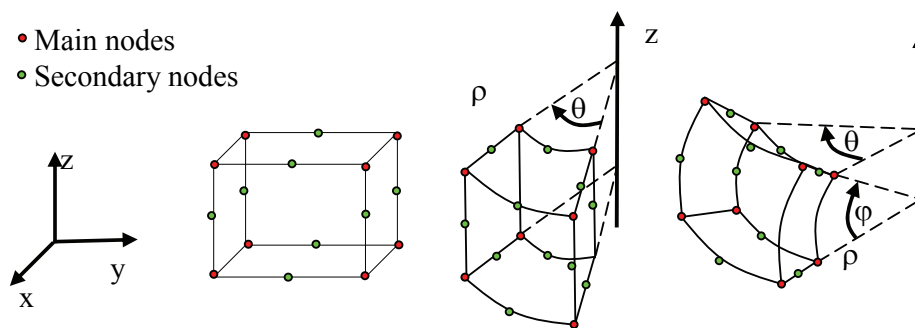


Fig. 4. Regular element

➤ Tetrahedral elements

The second geometry of elements is tetrahedral useful for mesh an intersection with two different regular geometry, cylindrical and cubic for example. The structure of this element is described by fig. 5 and the element is build with 4 or 9 nodes.

- Main nodes
- Secondary nodes

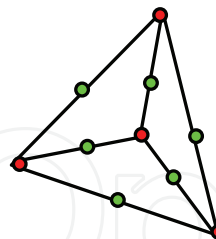


Fig. 5. Tetrahedral element

➤ Prism elements

The last geometry of elements is prism useful for mesh a centre of cylindrical geometry for example. The structure of this element is described by fig.6 and the element is build with 6 or 15 nodes.

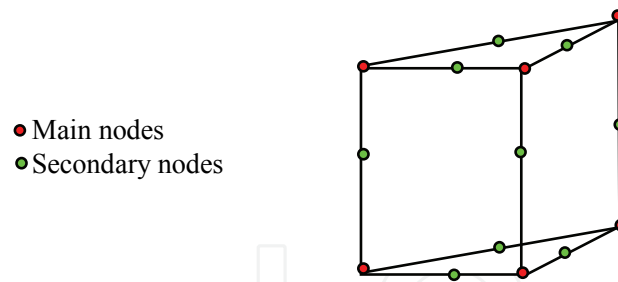


Fig. 6. Prism element

2.3 Building of laser welding process model

To build the laser welding process model, the main idea is to consider an electro-thermal model. The electrical part can give us a Gaussian distribution of the equipotential line. For simple application of electrical condition, we can simulate a Gaussian spatial distribution of equipotential. Using an adapted electrical conductivity, the thermal heat, caused by potential different between two isopotential, has also a Gaussian distribution. Then it is very simple and optimum to elaborate an electrothermal model about laser welding process.

Fig. 7 presents the electrical boundary condition on the cubic volume around the real laser weld volume. The laser beam simulate has the same characteristics than one previously presented in fig.2. The boundary conditions of potential are ground for five face of cube as it shown in fig. 7. On the last face of cube, the punctual potential V_{YAG} is applied in the centre of the face $O(0,0,0)$. The meshing method must build node for this specific point O .

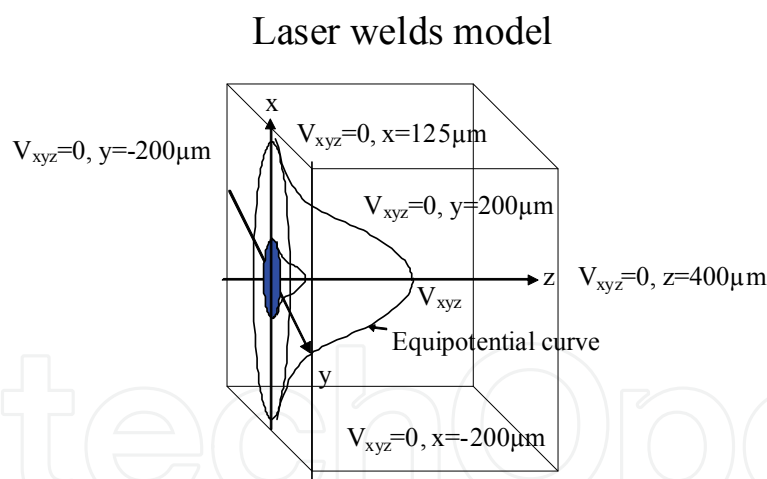


Fig. 7. Laser welding zone in electrical boundary conditions

The V_{LAS} potential is calculated using the thermodynamic relations of enthalpy ΔH based on the heat transfer and phase change. To simulate laser pulse energy E_{LAS} deposited on the surface of the laser welding zone, the V_{LAS} is also a pulse. The time whitening of the pulse Δt is related by the total power P_{LAS} deposited during the laser welding process. The relation between electrical model and thermal one is proposed in equation (5).

$$\Delta H = \frac{V_{LAS}^2}{R} \Delta t = mC_p \Delta T + mL_f \quad (5)$$

With m : the total mass of laser welded zone, C_p : the calorific capacity of material, L_f : the latent heat of material.

3. Modelling setup

3.1 Design of the laser module

Semiconductor Laser package bodies are typically either cylindrical-type or box-type styles. For light wave communication systems, box-type bodies are widely used and in particular Dual-In-Line or Butterfly packages with fibre pigtails. This study is focused on 1.55 μm Butterfly package Laser module and a technological description is presented in fig. 8. The DFB Laser diode (Distributed Feedback Laser diode InP/InGaAsP) emitting at 1.55 μm is soldered with a AuSn solder joint (8 μm) on the Laser submount (AlN), and then the submount is attached to the Laser platform (composed by a submount and 2 columns bearing the lens holder) in Kovar by a SnSb solder joint (8 μm). Lens 1, used to collimate the Laser beam from the Laser diode, and the isolator are welded to a lens holder (Kovar) by means of Nd:YAG Laser welding process.

The Laser platform and the lens holder are also welded corresponding to the sub-assembly 1. This last element is then attached to the thermoelectric cooler and mounted with a SnPbAg solder joint (10 μm) in a Butterfly-type package (Kovar). The sub-assembly 2 is composed of a second lens, used to focalized Laser beam into the fibre core, glued with an adhesive material into a circular ferule (Zirconia/Kovar). Finally, the sub-assembly 2 is Nd:YAG Laser welded to the Butterfly-type package providing a complete hermeticity for the system.

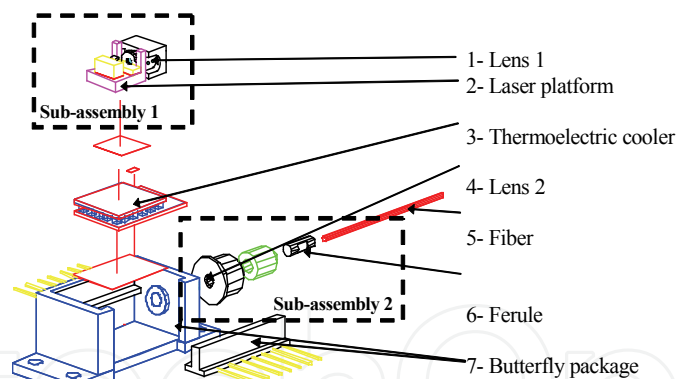


Fig. 8. Description of the Laser module showing the two main sub-assemblies

As an alternative to the common adhesives or solders used in the light-coupling process, Nd:YAG Laser welding offers a number of attractive features such as high weld strength to weld size ratio, minimal heat affected zone, reliability providing some benefits: low heat distortion, non-contact process, repeatability and ability to automate (Sherry and al., 1996). Nevertheless, the main drawback of Laser welding is that the intense energy input, resulting in severe thermal gradients, can contribute to generate strains driving elements out of alignment. Motions in excess of 10 μm can be thus introduced and submicron alignment usually requires some type of motion compensation after the initial welds to hold required tolerances (Hayashi and al., 1996).

3.2 Finite element analysis conditions

In order to calculate levels of stresses and strains after Nd:YAG Laser welding process between the Laser diode platform and the lens holder, FEM simulations are performed. Different models and boundary conditions are defined in this part. Sub-assembly 1 is composed of the Laser platform and the lens holder essentially in Kovar. The model is based on electrical, thermal and mechanical simulation using a multiphysics approach and will allow to extract isothermal contour plots to evaluate magnitude of thermal gradients in the sub-assembly 1. The final goal is to calculate residual stresses and the resultant optical beam axis deviation after this process.

Fig. 9-a presents the global model of sub-assembly 1 with a planar symmetry (Ox, Oy). Fixed points, considered as nodes without any degrees of freedom, represent fixing flanges used in manufacturing process to maintain the lens holder and the Laser platform during Laser welding process. The external loads are listed below:

- Weight is applied on the gravity centre,
- A Clamp forces F_{pres} are applied on the back of the lens holder during Laser welding process to guarantee an adjustment between Laser platform and lens holder,
- Laser heating boundary conditions are shown in fig. 9a and modeled by Joule heating considering the well-known thermal/electrical analogies. The equipotential surface is adjusted to obtain a maximum temperature at 1400 K. We use two different electrical characteristics to traduce a localized heat source as generated by a Nd:YAG Laser beam. This part will be developed in the next section.

Fig. 9 describes an optimized model with 7526 elements and 11803 nodes using three-dimensional tetrahedral multiphysics transfer elements was used for this sub-assembly 1 which is mainly composed of Kovar.

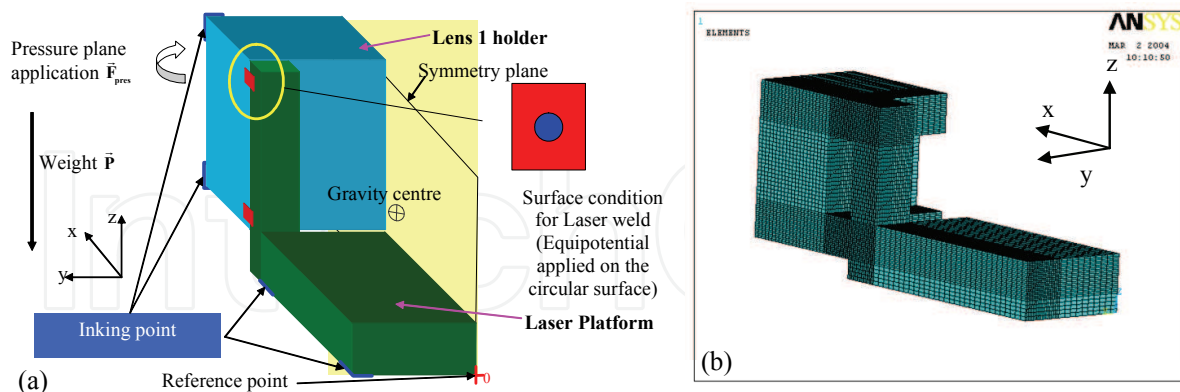


Fig. 9. Sub-assembly 1 simulated design with external loads (a), optimized FEM mesh model (b)

Material properties are assumed to be dependent on temperature (see table 1 below). The time dependence of Laser welding process has conducted us to run time-dependent (transient) simulations.

Fig. 10 summarizes the chronograms of pressure force, voltage of the top volume welded V_{YAG1} and voltage the bottom volume welded V_{YAG2} . On the top of fig. 10, we note the time

dependence of the thermal cartography analyses. In this study, the laser heating is modelled by Joule heating taking into account electrical/thermal energy considering that a Laser welded joint can be associated to an electrical resistance calculated from the same area of material (Kovar).

	Kovar		
	27°C	600°C	1200°C
CTE ($\mu\text{m}/^\circ\text{C}$)	5.13	5.86	11.5
Young modulus (GPa)	138	138	138
Yield strength (MPa)	345	245	50
Poisson ratio	0.317	0.317	0.317
Thermal conductivity ($\text{W}\cdot\text{m}^{-1}\cdot^\circ\text{C}^{-1}$)	17.3	17.3	17.3
Heat capacity ($\text{J}\cdot\text{kg}^{-1}$)	439	439	649
Melting point ($^\circ\text{C}$)		1450	

Table 1. Values of the material physical properties of Kovar using in sub-assembly 1 versus temperature

To evaluate the thermal energy developed in the volume of the welded joint, we considered the relation between the enthalpy variation and the electrical energy (6) :

$$\Delta H = \frac{V^2}{R} \Delta t \quad (6)$$

with ΔH defines the enthalpy variation, R is equivalent of an electrical resistance of the Laser welded joint volume, V corresponds to the time-dependent applied voltage (V_{YAG1} and V_{YAG2}) and Δt is the YAG Laser pulse duration (2.5 ms).

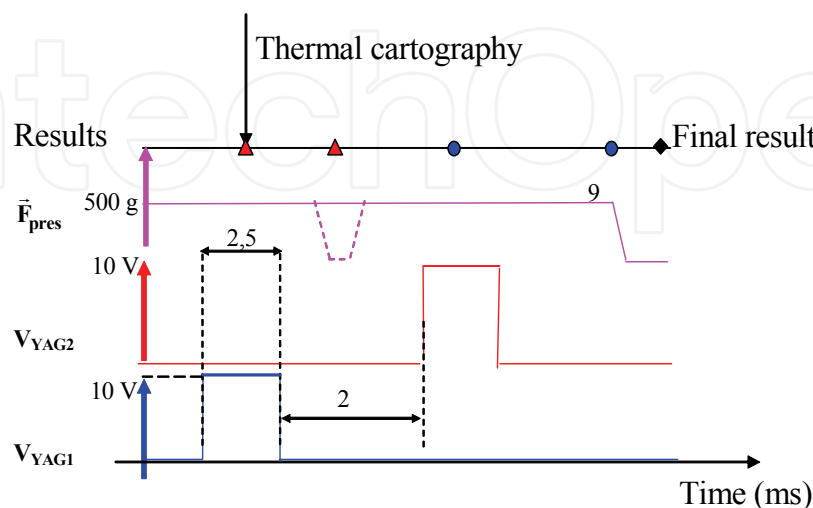


Fig. 10. Time dependence of boundary conditions for Sub-assembly 1

V_{YAG1} and V_{YAG2} correspond respectively to inferior and superior Laser welded joint and are not applied simultaneously as shown in fig. 10.

Deposited energy with a YAG Laser is calculated considering electrical energy dissipated from a resistance on which an applied voltage allows to simulate a thermal energy in the volume of the spot weld with a temperature close to the melting temperature. Our simulations are based on the following expressions giving the relation between electrical energy and thermodynamically conditions (7):

$$\frac{V^2}{R} \Delta t = mC_p \Delta T + L_f \quad (7)$$

$$\Delta H = mC_p \Delta T + L_s$$

Equations (7) give the heating conditions corresponding to the Laser energy quantity deposited on the material with C_p defines as heat capacity (in $J.kg^{-1}.\text{°C}^{-1}$) and L_f represents the latent heat of melting given in Joule. Cooling conditions taking into account of latent heat solidification L_s , given in Joule, are resumed by equation (3). It is known that, for Kovar, the heat capacity parameter has temperature dependence and literature allows to extract the value until 1200°C rather than heat latent of solidification which is difficult to obtain (Cheng and al., 1999). This parameter traduces cooling effect which is critical in this case. So proposed simulations are computed at a temperature close to 1473K corresponding to the temperature at which thermomechanical constants are given in table 1. All thermomechanical properties have been used to simulate the Laser welding process and give thermal and mechanical solutions.

4. Results and discussions

4.1 Thermomechanical simulations

Nd:YAG Laser welding process involves a highly focused Laser beam responsible of a non-uniform temperature distribution on the focus point. Simulated energy deposited allows being close to melting temperature of Kovar material (1473K). Fig. 11 shows the nodal solution contour plot of thermal cartography of Laser platform after first Laser welding process.

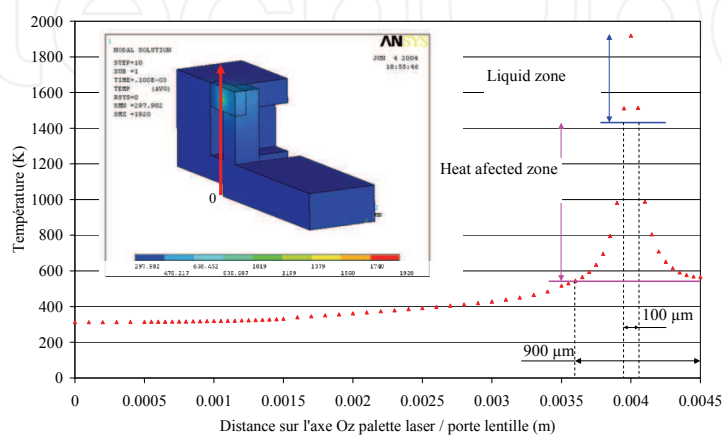


Fig. 11. Variation of the temperature along the column of the Laser submount

The temperature variation along the column of Laser platform can be fitted by a Gaussian law expressed as equation (8):

$$T(r) = T_1 + (T_0 - T_1) \exp(-r^2/W_0^2) \quad (8)$$

With $T_0 = 1427\text{K}$, the maximal temperature of Laser weld, $T_1 = 600\text{K}$ the minimal temperature of Laser weld and W_0 the beam waist defined as the minimum radius of the Laser beam.

Experimental and calculated beam waist values are the same and evaluated around $150 \mu\text{m}$ (Deshayes and al., 2003). The good agreement between experimental and calculated values validate the simulation approach for Laser Nd:YAG welding process.

Fig. 12 compares strains in sub-assembly 1 structure before and after Nd:YAG Laser welding process. Strain occurring in the column is observed and this particular view (deformed and no deformed nodal solution plots) allows highlighting optical beam axis deviation of the lens holder.

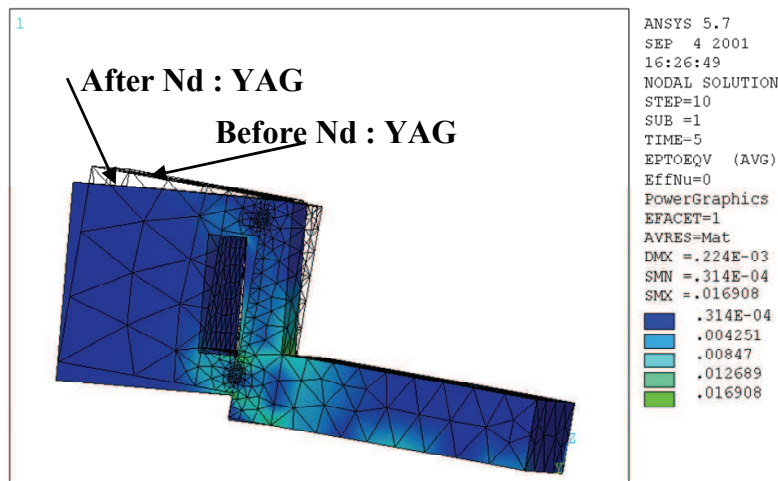


Fig. 12. Residual effective strains deformed and undeformed view located in sub-assembly 1

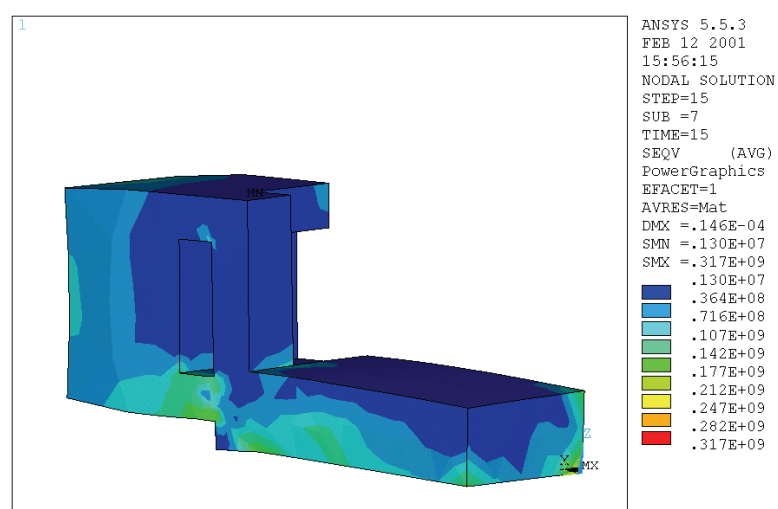


Fig. 13. Residual effective Von Mises stress (Pa) after Laser welding on the sub-assembly 1

Fig. 13 clearly shows the residual effective Von Mises stresses close to 55 MPa located in the column base of the Laser Platform after Laser welding.

Thermal gradients ($\approx 1100\text{K}$) along columns of Laser platform induce maximal displacements close to $2\ \mu\text{m}$ located in the column base after Nd:YAG Laser welding process in manufacturing conditions and maximal strains of 0.05% (fig. 13). These displacements are observed by optical axis angular deviation θ and Δx , Δy and Δz axial deviations. Calculated values of previous parameters are obtained from simulation results.

In fig. 14, two nodes of lens holder representing optical axis have been considered. We also reported Δx , Δy , Δz and θ deviations of optical axis allowing to give its final position after total Laser welding process.

Considering this two nodes, optical axis deviation resulting from residual stress after Laser welds can be evaluated close to an angular deviation of $\theta = 0.03^\circ$ and axial deviations of $\Delta x_{\text{max}} = 2\ \mu\text{m}$, $\Delta y = 0$ and $\Delta z_{\text{max}} = 0.1\ \mu\text{m}$. Experimental analyses for evaluation of optical coupling drop in 1550 nm Laser modules have reported that optical power losses about 40 % result from two critical values of parameters variation:

- An angular deviation θ of 0.02° between sub-assembly 1 and sub-assembly 2,
- Δy , Δz deviations of $10\ \mu\text{m}$ between Laser diode and Lens holder.

At this step of the manufacturing process, optical coupling between lens holder and Laser diode is correct because Δy , Δz deviations are close to $0.1\ \mu\text{m}$ corresponding to optical coupling losses lower than 0.1%. Thus, an operator could not suspect a possible displacement of the first lens axis after Nd:YAG Laser welds. The assembling step between the pigtail and the sub-assembly 1 requires then a dynamic alignment to find maximal optical coupling. In this case, the operator can adjust a possible optical beam axis deviation without any information about the value of the previous deviation and the level of accumulated stresses trapped in the sub-assembly one.

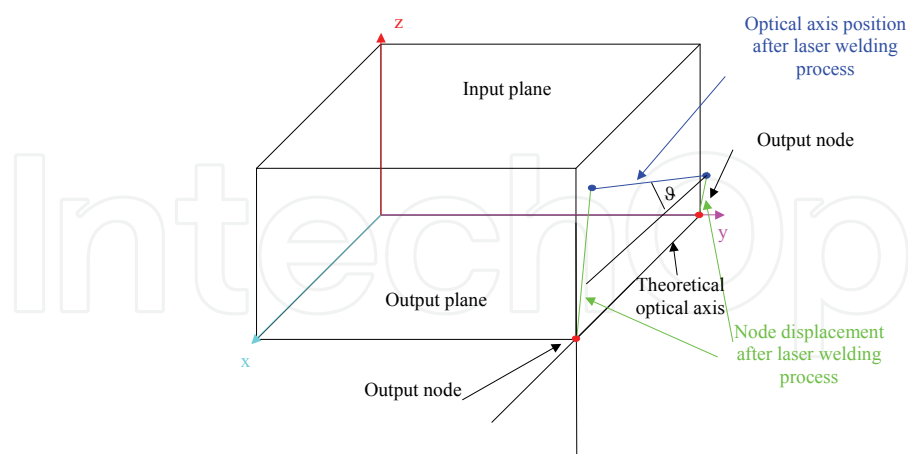


Fig. 14. Residual effective strains deformed and unreformed view located in sub-assembly 1

After Nd:YAG Laser welds, intrinsic and extrinsic stresses can appear. Intrinsic stresses are generally related to only Laser YAG energy deposition on metal surface. The most important accumulated stress is located inside the HAZ caused by huge plastic deformation and very rapid thermal variation in welded joints (Jang, 1996; Panin and al., 1998). Extrinsic

stresses are caused by external loads applied during process and discontinuity of materials on the interface (Inoue and Koguchi, 1997). In our case, the most important external load is represented by pressure strength F_{pres} used to ensure an adjustment between Laser platform and lens holder.

Relaxation of accumulated stresses in the sub-assembly 1 can occur and could be accelerated by defects induced in the welded zone (Inoue and Koguchi, 1997; Hariprasad, Sastry and Jerina). Rapid solidification processing in HAZ leads to a metastable phase formation, solid solution or dispersion strengthened alloys and intermetallics and the whole physical phenomenon is at the origin of defects formation located in welded joints (Hariprasad, Sastry and Jerina; Cheng and Wang, 1996). It has demonstrated that metallic alloys creep fatigue is related to defects rate located in welded joints considered as a metallic alloy zones (Asayama, 2000). In particular, a model based on molecular dynamics calculations, developed by J.D. Vazquez, has discussed on isotropic and anisotropic relaxation phenomenon from simulations of lattice relaxation of metallic alloys considering the sudden appearance of vacancy or an interstitial site in the crystal (Dominguez-Vazquez, 1998). This microscopic relaxation model allows highlighting macroscopic effective displacement of system responsible of relaxation phase. Experimental measurements, using in particular an optical method, have been also conducted to observe strains, stresses and fractures of welded joints at the mesoscale level (Panin and al., 1998). This study has characterized, in bulk material, the accumulated stresses located in HAZ and their evolution after Laser welding process. So our interpretation of gradual optical power drift between the sub-assembly 1 and the pigtail can be explained by relaxation phenomenon and time evolution can be directly related to the number and the location of defects into the welded joints but also in the structure.

Experimental procedure has been established to localize strains and stresses in sub-assembly 1 during the whole step Nd:YAG Laser welding process and evaluation of relaxation phenomenon after thermal cycles.

4.2 Ageing tests analysis

Qualification procedures, in particular power drift measurement, must be conducted to validate the system with respect to tolerances through temperature cycles or storage temperature characterizing the limits and the margins of the technology. Actual standards tend to be 500 cycles in the temperature range $-40^{\circ}\text{C}/+85^{\circ}\text{C}$ with a failure criterion of 10% of optical power drift. The methodology of failure diagnostic for optoelectronics components and modules for telecommunication applications imposed to do ageing tests to validate different assumptions coming from the simulation results. The detailed of this procedure is presented by (Y. Deshayes and al., 2003).

First ageing tests have been made on 1550 nm InGaAsP/InP DFB Laser diodes. After 500 thermal cycles $-40^{\circ}\text{C}/+85^{\circ}\text{C}$, no failure occurred on Laser diodes. Measurements have been made with a specific test bench with temperature dependence has been developed to monitor $P(I)$, $I(V)$ and $L(E)$. This result demonstrates that optical power drift is only associated to misalignment in relation with thermomechanical aspects. The second ageing test is made on nine different optoelectronic modules in final packaging. Fig. 13 shows variations of ΔE_{ta} (%) defined by :

$$\Delta E_{ta} = \left[\frac{\Delta P_{opt}}{P_{opt}} \right]_{I=100mA} \quad (9)$$

with P_{opt} is initial optical power measurement of the laser module, ΔP_{opt} is the difference between optical power measured after ageing time and initial optical power measurement and I is the current value for optical power measurement.

This experimental procedure has been applied on nine InGaAsP/ InP 1550 nm Laser modules (LM1 to LM9) versus thermal cycles $-40^{\circ}\text{C}/+85^{\circ}\text{C}$. In fig. 8, evolution of ΔE_{ta} (%) measured at 100 mA from 0 to 500 thermal cycles ($-40^{\circ}\text{C}/+85^{\circ}\text{C}$) are reported. Experimental and simulation results lead to give failure modes and assumptions on failure location (Deshayes and al., 2003):

- sudden total optical power drop explained by a break located in the optical fibre core,
- gradual optical power drift outside the failure criteria limit in relation with thermomechanical aspect responsible of columns deformation in sub-assembly 1 and related by stresses relaxation phenomenon,
- gradual optical power drift inside the failure criteria demonstrating the relative instability of optical coupling in Laser module especially on sub-assembly 1.

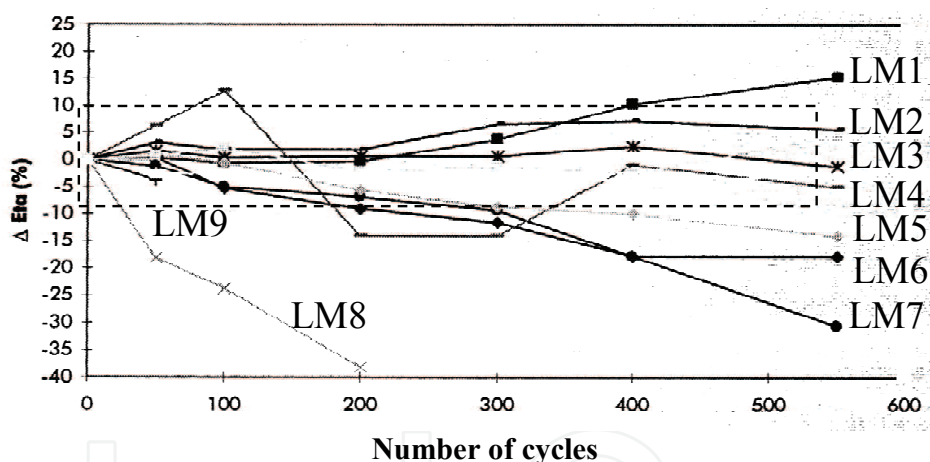


Fig. 15. Ageing test results on 1550 nm InGaAsP/InP Laser module

4.3 Optical misalignment using process dispersion

The new method proposed in the introduction of this paper corresponds to an evolution of optoelectronic qualification practices needing to develop new working methods than the usual "go-no go" qualification tests. The final objective is to define relevant tests performed to define "generic" accelerated test and assess both robustness and reliability of the component. In this case, technological dispersion modelling represents an attractive tool to identify the effect of a critical technological parameter on the optical deviation distribution and reduce time duration of tests. Among these parameters, we can list: material properties, geometric dimensions, welding and solder processes...

Fig. 13 reveals the difference of behaviour between optical modules in term of optical coupling deviations, could be related to manufacturing process dispersion. As we have yet

demonstrated, the most sensitive manufacturing process is Nd:YAG Laser welding associated to clamp forces F_{pres} and Laser heating conditions (E_0). Until now, 3D FEM simulations have been performed considering F_{pres} and E as average constant values called F_{pres0} and E_0 . The range of these last parameters is limited by manufacturing process. The parameter F_{pres} is set from $F_{pres0} \pm 20\%$ and laser Nd:YAG energy from $E_0 \pm 20\%$ according with manufacturer specification (Gibet, 2001).

In the case of clamp force F_{pres} variation limited by $F_{pres0} \pm 20\%$, less than 10^{-5} degree on angular deviation is observed and stresses stay constant. For this configuration, the impact of clamp force variations on the optical coupling efficiency could be considered as negligible.

The Laser Nd:YAG energy E corresponds to the one absorbed by the welded joint. The amplitude of dispersion can be correlated both to the reflectance of the Laser impact area and thickness of gold deposited on the Kovar mainly composing the sub assembly 1. The absorbance of Laser energy is related to the thickness of gold, water concentration and roughness of the material surface (Watanabe and al., 2004; Martin, Blanchard and Weightman, 2003; Zhang, 2004). The thin film of gold allows to adsorbed infrared $1\mu\text{m}$ wavelength laser Nd:YAG beam.

Fig. 16 reports variations of optical angular deviation versus energy of the Laser beam. In the same time, we report the maximal stress located in top welded zones. The global study indicates that welding zone is the most critical zone, so FEM simulation has been optimized to precise stresses in welding zone. After specific analyses, we identify that top welding zone is the most critical zone and amplitude of stress is optimized. The energy variation is the experimental data given by manufacturer. It is shown that higher is the energy deposited on the welded zone, higher is the stress level but lower is the optical deviation. This key result is closely correlated with results reported by W.H. Cheng (Jerina; Cheng and Wang, 1996). The displacement is critical because $2/100^\circ$ induces 40 % of optical power losses and explain the magnitude of ΔE_{ta} (%) shows in fig. 8. The drift of stresses and displacements versus energy E/E_0 is weak and indicates that energy level of Nd: YAG cannot be adjusting to reduce the optical misalignment. So, this key result indicates that the architecture of the system should be optimized to reduce the impact of laser welding process on the optical misalignment.

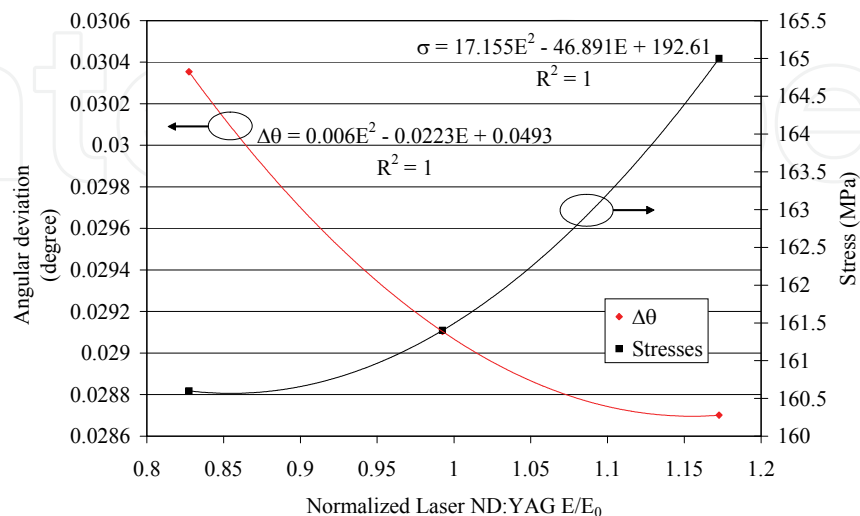


Fig. 16. Optical angular deviation and stresses accumulated versus energy laser Nd:YAG

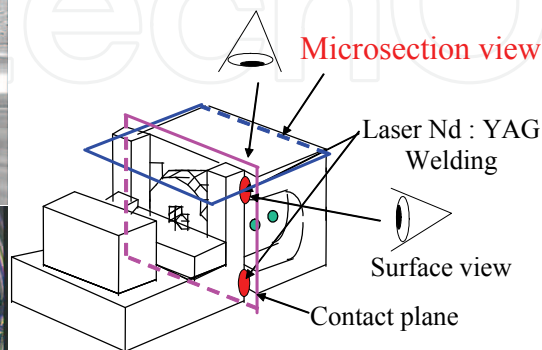
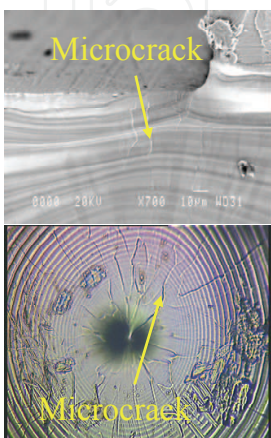
The different behaviour of different modules shows in fig.16 can be explained by the initial stresses and displacements. This phenomenon is associated to the fact that laser submount and lens support are hyper static system. The methodology presented in this paper conduct manufacturer to modified the design of laser submount taking into account all these results. The new optical module are now qualified using the same standard requirements for telecommunication applications.

5. Conclusion and perspectives

Laser welding process in sub-assembly 1 has been identified as the most potential critical zone and to correlate simulation results using ANSYS software, experimental analyses have been also investigated (Deshayes, Béchou and Danto, 2001).

Calculated optical misalignment in sub-assembly 1 have demonstrated an angular optical beam axis deviation of 0.03° and responsible of a possible first lens axis movement confirming that Laser welding process can induce optical instability of Laser modules and degradation of performances for telecommunication applications. The main solution could be given by a better optimization of the Nd:YAG Laser power density close to $1.5 \cdot 10^5$ W/cm². For this technology, average Nd:YAG Laser power density reaches $2.5 \cdot 10^5$ W/cm² and can generate bulk defects and thermal stresses in welded joints (fig. 17). W.H. Cheng has established that optical losses in Laser modules can relate to the presence of bulk fractures (Jerina; Cheng and Wang, 1996). It has also been highlight that power density is responsible of bulk defects and accumulative stresses. In our case, the presence of bulk defects, observed in fig. 17, could explain random acceleration of time stress relaxation allowing optical power decrease. The time before failure corresponding to $\pm 10\%$ of the optical power drift is directly related to the manufacturing process and to the order of static non determination from a mechanical point of view of the system strongly dependent on the Laser platform and the lens holder design. All conditions are correlated to a mechanical misalignment between Lens axis and pigtail. The major cause of bulk defects formation in the Laser welding process for sub-assembly 1 is due to the excess Laser energy. The other causes are gas bubbles trapped within the weld sections and the heterogeneous nucleation in welded joints (Jerina; Cheng and Wang, 1996).

Surface defects



Bulk defects

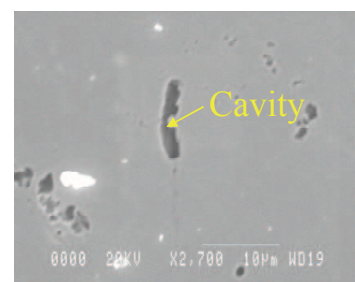


Fig. 17. Bulk defects formation in a Laser weld joint

This chapter reports 3D thermomechanical simulations and experimental tests in order to identify critical zones in a Butterfly-package Laser module showing that three main zones must be carefully analyzed: shape and volume of glue in the ferrule, solders and, in particular, Laser welds. Laser welding process is a useful and effective method to ensure hermeticity and secure metal parts but the mechanical distortions due to severe thermal gradients should be controlled within allowance limits. The accumulated stresses are close to 160 MPa in welded zones. The main advantages of this technique are given by precision of alignment close to $\pm 0.2 \mu\text{m}$, the whole process fully automated to contain the cycle's time within 60 to 90 seconds. But it has been shown that one of the main inconvenient of the Laser welding process is the excess of deposited Laser energy resulting in high thermal gradients (700 K on $200 \mu\text{m}$) and residual stresses (around 160 MPa) in the Laser platform responsible of an optical misalignment and a possible failure in terms of optical power drift requirements. We have demonstrated that FEM simulations, to predict distortion of Laser welding which is very difficult to measure, is very attractive and can be applied to different package configurations.

Such a study is attractive for the definition of more realistic and optimized realistic life cycle profiles, taking advantages of previous methodologies already experienced in the field of microelectronics or military industries.

Experimental failure analyses will be also conducted to validate thermomechanical simulations, focused in particular on Laser welded joints in order to propose assumptions for accumulated strains relaxation phenomenon. In this context, both thermal, electrical and thermomechanical simulations on the package must be realized using an original approach based on multiphysics computations of ANSYS software, in particular for electro-thermal Nd:YAG Laser modelling (Fricke, Keim and Schmidt, 2001). First, a description of the Laser module is given and 3D-FEM models of each sub-assembly are presented taking into account of the different materials characteristics versus temperature and external loads related to manufacturing steps. The last section gives simulation results of the main sub-assemblies of the Laser module concluding on thermomechanical sensitivity of critical zones and the impact on a possible optical axis misalignment.

Our activities are now focused on FEM predictions that could be improved by a detailed knowledge of the effect of bulk defects located in Laser welded joints on stresses relaxation phenomenon and also by a better implementation of heating and cooling conditions in computations. The final objective is to improve packaging design rules and optical misalignment reduction in order to achieve highly reliable bandwidth single mode fibre communication systems.

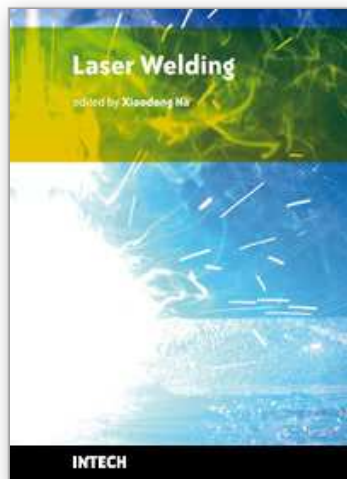
6. References

- Asayama (2000). Creep fatigue evaluation of stainless steel welded joints in FBR class 1 components. *Nuclear Engineering and Design*, 198, 2, (February 2000), pp. 25-40, ISSN: 00295493
- Breedis (2001). Monte Carlo tolerance analysis of a passively aligned silicon waferboard package, *Proceeding of Electronic Components and Technology Conference*, pp. 247-254, ISBN: 05695503, United States, 29 May 2001 through 1 June 2001, IEEE, Orlando
- Cheng and al. (1999) Thermal stresses in box-type Laser packages, *Optical and Quantum Electronics*, 31, 4 (April 1999), pp. 293-302, ISSN: 03068919

- Deshayes, Béchou and Danto (2001). Experimental validation of thermomechanical simulations on 1550 nm Laser modules, *Internal Report, ALCATEL Optronics-IXL*, September 2001.
- Deshayes and al. (2003). Three-dimensional FEM simulations of thermomechanical stresses in 1.55 μm laser modules, *Microelectronics Reliability*, 43, 7, (July 2003), pp. 1125-1136. ISSN: 00262714
- Dominguez-Vazquez and al. (1998). Relaxation of metals: A model based on MD calculations. *Nuclear Instruments and Methods in Physics Research, Section B: Beam Interactions with Materials and Atoms*, 135, 1-4, (February 1998), pp. 214-218, ISSN: 0168583X
- Fricke, E. Keim and J. Schmidt (2001). Numerical weld modeling-method for calculating weld-induced residual stresses, *Numerical engineering and design*, 206, 2-3, (June 2001), pp. 139-150, ISSN: 00295493
- Gibet (2001). Procédure de fabrication de têtes optique, Alcatel Optronics - France, Research and development department, Internal report, 2001.
- Goudard and al. (2002). New qualification approaches for opto-electronic devices, *52nd Electronic Components and Technology Conference*, pp. 551-557, ISBN: 05695503, United States, 28 May 2002 through 31 May 2002, IEEE, San Diego
- Hariprasad, Sastry and Jerina (1996). Deformation behavior of a rapidly solidified fine grained Al-8.5%Fe-1.2%V-1.7%Si alloy, *acta Materialia*, 44, 1, (January 1996), pp. 383-389, ISSN: 13596454
- Hayashi and Tsunetsugu (1996). Optical module with MU connector interface using self-alignment technique by solder-bump chip bonding, *Proceedings of the 1996 IEEE 46th Electronic Components & Technology Conference*, pp. 13-19, ISBN: 05695503, United States, 28 May 1996 through 31 May 1996, IEEE, Orlando
- Inoue and Koguchi (1997). Relaxation of thermal stresses in dissimilar materials (approach based on stress intensity), *International Journal of Solids and Structures*, 34, 25, (September 1997), pp. 3215-3233, ISSN: 00207683
- Jang (1996). Packaging of photonic devices using Laser welding, *Proceedings of SPIE - The International Society for Optical Engineering*, pp. 138-149, ISBN: 0819419745, United States, 25 October 1995 through 26 October 1995, Society of Photo-Optical Instrumentation Engineers, Philadelphia
- Martin, Blanchard and Weightman (2003). The effect of surface morphology upon the optical response of Au(1 1 0), *Surface Science*, 532-535, (10 June 2003), pp. 1-7, ISSN: 00396028
- McLeod and al. (2002). Packaging of micro-optics component to meet Telcordia standards, *Proceeding of Optical Fiber Communication Conference and Exhibit*, pp. 326-327, United States, 17 March 2002 through 22 March 2002, IEEE, Anaheim
- Panin and al. (1998). Relaxation mechanism of rotational type in fracture of weld joints for austenitic steels, *Theoretical and Applied Fracture Mechanics*, 29, 2, pp. 99-102, ISSN: 01678442
- Sherry and al. (1996). High performance optoelectronic packaging for 2.5 and 10 Gb/s Laser modules, *Proceeding of Electronic Components and Technology Conference*, pp. 620-627, ISBN: 05695503, United States, 28 May 1996 through 31 May 1996, IEEE, Orlando

- Song and al. (1996). Laser weldability analysis of high-speed optical transmission device packaging, *IEEE Transaction on Component, Packaging and Manufacturing Technology*, 19, 4, (November 1996), pp. 758-763, ISSN: 10709894
- Watanabe and al. (2004) Optimizing mechanical properties of laser-welded gold alloy through heat treatment, *Dental Materials*, 20, 7, (September 2004), pp. 630-634, ISSN: 01095641
- Zhang and al. (2004). Relationship between weld quality and optical emissions in underwater Nd: YAG laser welding, *Optics and Lasers in Engineering*, 41, 5, (May 2004), pp. 717-730, ISSN: 01438166

IntechOpen



Laser Welding

Edited by Xiaodong Na, Stone

ISBN 978-953-307-129-9

Hard cover, 240 pages

Publisher Sciyo

Published online 17, August, 2010

Published in print edition August, 2010

This book is entitled to laser welding processes. The objective is to introduce relatively established methodologies and techniques which have been studied, developed and applied either in industries or researches. State-of-the art developments aimed at improving or next generation technologies will be presented covering topics such as monitoring, modelling, control, and industrial application. This book is to provide effective solutions to various applications for field engineers and researchers who are interested in laser material processing.

How to reference

In order to correctly reference this scholarly work, feel free to copy and paste the following:

Yannick Deshayes (2010). Laser Welding Process: Characteristics and FEM Simulations, Laser Welding, Xiaodong Na, Stone (Ed.), ISBN: 978-953-307-129-9, InTech, Available from:

<http://www.intechopen.com/books/laser-welding/laser-welding-process-characteristics-and-fem-simulations>

INTECH
open science | open minds

InTech Europe

University Campus STeP Ri
Slavka Krautzeka 83/A
51000 Rijeka, Croatia
Phone: +385 (51) 770 447
Fax: +385 (51) 686 166
www.intechopen.com

InTech China

Unit 405, Office Block, Hotel Equatorial Shanghai
No.65, Yan An Road (West), Shanghai, 200040, China
中国上海市延安西路65号上海国际贵都大饭店办公楼405单元
Phone: +86-21-62489820
Fax: +86-21-62489821

© 2010 The Author(s). Licensee IntechOpen. This chapter is distributed under the terms of the [Creative Commons Attribution-NonCommercial-ShareAlike-3.0 License](#), which permits use, distribution and reproduction for non-commercial purposes, provided the original is properly cited and derivative works building on this content are distributed under the same license.

IntechOpen

IntechOpen